

## Engineering Correlation Effects via Artificially Designed Oxide Superlattices

Hanghui Chen,<sup>1,2</sup> Andrew J. Millis,<sup>1</sup> and Chris A. Marianetti<sup>2</sup>

<sup>1</sup>*Department of Physics, Columbia University, New York, New York 10027, USA*

<sup>2</sup>*Department of Applied Physics and Applied Mathematics, Columbia University, New York, New York 10027, USA*

(Received 29 April 2013; published 10 September 2013)

*Ab initio* calculations are used to predict that a superlattice composed of layers of LaTiO<sub>3</sub> and LaNiO<sub>3</sub> alternating along the [001] direction is a  $S = 1$  Mott insulator with large magnetic moments on the Ni sites, negligible moments on the Ti sites and a charge transfer gap set by the energy difference between Ni  $d$  and Ti  $d$  states, distinct from conventional Mott insulators. Correlation effects are enhanced on the Ni sites via filling the oxygen  $p$  states and reducing the Ni-O-Ni bond angle. Small hole (electron) doping of the superlattice leads to a two-dimensional single-band situation with holes (electrons) residing on the Ni  $d_{x^2-y^2}$  (Ti  $d_{xy}$ ) orbital and coupled to antiferromagnetically correlated spins in the NiO<sub>2</sub> layer.

DOI: [10.1103/PhysRevLett.111.116403](https://doi.org/10.1103/PhysRevLett.111.116403)

PACS numbers: 71.27.+a, 71.10.Fd, 74.78.Fk

Recent advances in atomic scale oxide synthesis provide new approaches to creating novel electronic and magnetic states in artificially designed heterostructures [1]. Pioneering discoveries include a quasi-two-dimensional conducting electron gas at insulating oxide interfaces [2–6], thickness dependent or strain-induced metal-insulator transition in ultrathin films [7–10] and at inserted monolayers [11], as well as emergent magnetism [12–15], orbital reconstruction [16–18] and pseudogap [19]. These discoveries mark important milestones towards the goal of using the new synthesis capabilities to engineer correlation effects such as magnetism and superconductivity.

In this Letter, we use *ab initio* electronic structure methods to demonstrate the viability of internal charge transfer and heterostructuring as a route to controlling correlation effects in complex oxides. The calculations indicate that a superlattice composed of layers of LaTiO<sub>3</sub> (a narrow gap  $S = 1/2$  antiferromagnet) and LaNiO<sub>3</sub> (a wideband paramagnetic metal) is a  $S = 1$  charge transfer Mott insulator, with magnetic moments on the Ni sites, negligible magnetism on the Ti sites, and a charge transfer gap controlled by the energy difference between the Ni and Ti  $d$  levels, which is distinct from conventional  $S = 1$  Mott insulators (e.g., NiO and La<sub>2</sub>NiO<sub>4</sub>). We further show that small hole doping may lead to a two-dimensional single-band Fermi surface, with carriers residing on the Ni  $d_{x^2-y^2}$  orbital and strongly coupled to correlated spins on the Ni  $d_{3z^2-r^2}$  orbital, whereas doping with electrons also leads to a two-dimensional Fermi surface but with carriers on the Ti  $d_{xy}$  orbital and weakly coupled to antiferromagnetic ordering in the NiO<sub>2</sub> layer.

Charge transfer at oxide interfaces has been previously considered, for example, in the context of propagation of magnetic order from a manganite to a cuprate material [20,21], or titanate [22], or nickelate [23–25]. Here we show that the charge transfer can be large enough to fundamentally change the electronic properties. In the superlattice considered here, the lone electron in the

conduction bands of the TiO<sub>2</sub> layer is completely depopulated and the NiO<sub>2</sub> layer is transformed from a wideband metal to a  $S = 1$  Mott insulator.

Formal valence changes are also known in related materials, for example,  $A_2BB'O_6$  double perovskites, which can be viewed as a [111] direction superlattice [26]. Experimental indications of formal valence changes have been reported for La<sub>2</sub>MnNiO<sub>6</sub> [27] and La<sub>2</sub>TiCoO<sub>6</sub> [28], but these systems seem not to have been the subject of systematic theoretical studies. Here we provide a comprehensive theoretical analysis of this phenomena in the context of a different and more easily synthesized [001] superlattice. An important feature of the [001] superlattice not found in double perovskites is an orbital ordering [29,30] with Ni  $d_{x^2-y^2}$  at the valence band maximum and Ti  $d_{xy}$  at the conduction band minimum. This orbital ordering leads to a strongly two-dimensional character for doped holes and electrons which are coupled to correlated spins in the NiO<sub>2</sub> layer.

To understand the origin of charge transfer and formal valence changes, we sketch the band structure of the (LaTiO<sub>3</sub>)<sub>1</sub>/(LaNiO<sub>3</sub>)<sub>1</sub> superlattice in Fig. 1(a). We begin with bulk LaTiO<sub>3</sub>, where the nominal electronic configuration involves one electron in Ti  $d$  states ( $d^1$ ), which lie well above the filled oxygen  $p$  states. Bulk LaNiO<sub>3</sub>, on the other hand, has a nominal electronic configuration of Ni  $d^7$  with six electrons filling up the  $t_{2g}$  shell and one electron in the  $e_g$  orbitals, which overlap in energy with the oxygen  $p$  states. The different electronegativities of Ti and Ni suggest that in a superlattice, the Ti  $d$  electron may be transferred to the NiO<sub>2</sub> plane, leading to a new nominal electronic configuration: Ti  $d^0$  + Ni  $d^8$ , with strongly enhanced correlations arising from the half filling of the Ni  $e_g$  shell.

To quantitatively test the above idea of engineering correlation effects via charge transfer and explore the predicted phenomena, we performed density functional theory (DFT) plus  $U$  calculations (DFT +  $U$ ) including fully structural relaxations (see Supplemental Material

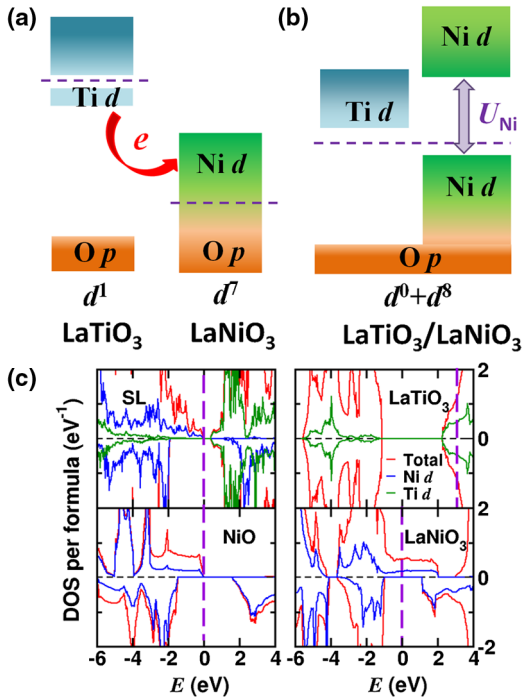


FIG. 1 (color online). (a) Schematic band structures of component materials  $\text{LaTiO}_3$  and  $\text{LaNiO}_3$ . The dashed purple lines are the Fermi levels for the two materials.  $\text{LaTiO}_3$  shows insulating behavior with a small excitation gap set by  $\text{Ti } d$ - $d$  transitions and a wide energy separation between  $\text{Ti } d$  states and  $\text{O } p$  states.  $\text{LaNiO}_3$  exhibits metallic behavior with strong mixing between  $\text{Ni } d$  states and  $\text{O } p$  states. The red arrow highlights the direction of charge transfer in the superlattice. (b) Schematic band structure of the  $(\text{LaTiO}_3)_1/(\text{LaNiO}_3)_1$  superlattice.  $\text{Ti } d$  states are above the Fermi level (dashed purple line). Correlation effects split  $\text{Ni } d$  states into lower and upper Hubbard bands, separated by  $U_{\text{Ni}}$ . (c) Densities of states for majority (above axis) and minority (below axis) spins of superlattice (upper left) and reference materials  $\text{NiO}$  (lower left),  $\text{LaTiO}_3$  (upper right; zero of energy is shifted so that oxygen bands align with those of  $\text{LaNiO}_3$ ) and  $\text{LaNiO}_3$  (lower right). The densities of states are obtained using DFT +  $U$  calculations with  $U_{\text{Ni}} = 6$  eV and  $U_{\text{Ti}} = 4$  eV.

[31] for details). The unit cell used in the simulations is shown in Fig. 2. We considered ferromagnetic ( $F$ ), stripe antiferromagnetic [ $S$ , wave vector  $(0, 1/2)$ ] and checkerboard antiferromagnetic [ $G$ , wave vector  $(1/2, 1/2)$ ] states, and several values of  $U$ . The main conclusions are found to be independent of the nature of the magnetic order and the value of  $U$  (provided that  $U$  is within a physically reasonable range). The upper left panel of Fig. 1(c) shows the density of states (DOS) of the superlattice calculated using the physically reasonable values  $U_{\text{Ni}} = 6$  eV and  $U_{\text{Ti}} = 4$  eV [32]; the ferromagnetic phase is chosen for clarity of presentation. The bands corresponding to the majority spin  $\text{Ni } d$  states are fully occupied, while those corresponding to  $\text{Ti } d$  states are empty, indicative of a nominal  $\text{Ti } d^0 + \text{Ni } d^8$  configuration. The superlattice is insulating, with a 0.4 eV energy gap; the highest occupied states are  $\text{Ni } d$  states; the

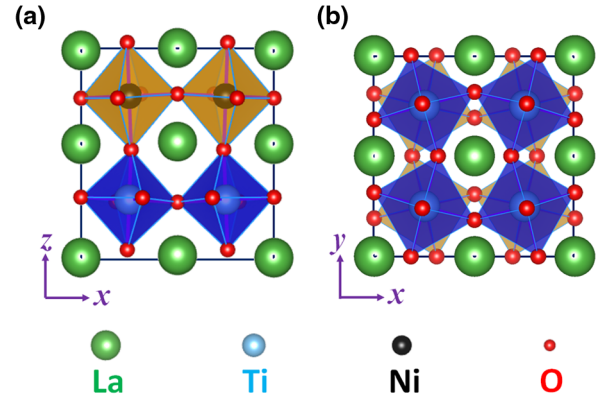


FIG. 2 (color online). Side view (a) and top view (b) of the unit cell of the  $(\text{LaTiO}_3)_1/(\text{LaNiO}_3)_1$  superlattice simulated here. The atom positions are obtained from a representative relaxed structure found in our first-principles calculations. La atoms are green, Ti atoms are blue, Ni atoms are black, and O atoms are red. The oxygen octahedra, shaded orange, enclose Ni atoms and the oxygen octahedra, shaded dark blue, enclose Ti atoms. The side view (a) shows a weak tilting of oxygen octahedra. The top view (b) highlights a strong rotation of oxygen octahedra.

lowest unoccupied states are  $\text{Ti } d$  states. The energy gap to the  $\text{Ni}$  unoccupied  $d$  states is much larger, around 1.5 eV.

The other panels of Fig. 1(c) show the densities of states calculated within the same scheme for three reference materials: face-centered  $\text{NiO}$  (lower left), cubic perovskite  $\text{LaTiO}_3$  (upper right, note shift in energy axis), and cubic perovskite  $\text{LaNiO}_3$  (lower right). We see that the superlattice DOS strongly resembles that of  $\text{NiO}$ , except with  $\text{Ti } d$  states added in the middle of the  $\text{NiO}$  insulating gap. The densities of states of the two constituents  $\text{LaNiO}_3$  and  $\text{LaTiO}_3$  [right panels of Fig. 1(c); note the shift in Fermi levels] are strikingly different.  $\text{LaNiO}_3$  is metallic, with a large density of non- $\text{Ni}$  (in fact oxygen) states in the vicinity of the Fermi surface.  $\text{LaTiO}_3$  has partially occupied  $\text{Ti } d$  states. The dramatic difference in densities of states between the superlattice [upper left panel of Fig. 1(c)] and the constituent materials [right panels of Fig. 1(c)] shows that an electronic reconstruction has taken place. (Note that in our calculations  $\text{LaTiO}_3$  is metallic because we have assumed cubic symmetry. A similar calculation but using the experimental structure for bulk  $\text{LaTiO}_3$  produces insulating behavior with a small energy gap [33]. However, the energy separation between the  $\text{Ti } d$  and  $\text{O } p$  states remains about 3 eV, no matter whether the small gap is opened or not at the Fermi level, which thus does not affect the charge transfer picture.) With  $\text{O } p$  states of the two materials aligned [see the right panels of Fig. 1(c)], the lowest occupied  $\text{Ti } d$  states are about 2 eV higher than the highest occupied  $\text{Ni } d$  states, which is the driving force for the electronic reconstruction, consistent with the schematics shown in panel (a) of Fig. 1. We mention here that the actual charge transfer, which we have computed from the  $z$  dependence of the full DFT charge density (see Supplemental Material [31]), is only

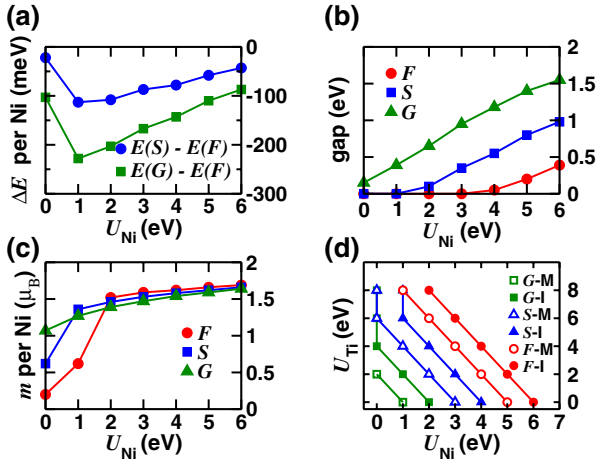


FIG. 3 (color online). Panels (a)–(c): Electronic and magnetic properties of the  $(\text{LaTiO}_3)_1/(\text{LaNiO}_3)_1$  superlattice for different magnetic orderings ( $F$  denotes ferromagnetic ordering,  $S$  denotes  $S$ -type or stripe antiferromagnetic ordering, and  $G$  denotes  $G$ -type or checkerboard-patterned antiferromagnetic ordering) as a function of  $U_{\text{Ni}}$  with  $U_{\text{Ti}} = 4$  eV. (a) Energy difference per Ni between different magnetic orderings. (b) Minimum excitation gap. (c) Absolute value of site projected magnetization of Ni  $d$  states. (d) Metal-insulator boundaries for each magnetic ordering on the  $(U_{\text{Ni}}, U_{\text{Ti}})$  phase diagram, respectively.  $F$ ,  $S$ , and  $G$  have the same meaning as in (a)–(c). “ $M$ ” and “ $I$ ” denote metallic and insulating states. The open symbols denote the upper limits of  $U_{\text{Ni}}$  for which metallic phases are found, while the solid symbols indicate the lower limits of  $U_{\text{Ni}}$  for which insulating phases have been found (note that only integer values of  $U$  have been studied).

$\sim 0.2$  electron per Ni rather than one electron per Ni as inferred from the formal valence changes, because the charge transfer in the near Fermi surface states is to a large degree compensated by rehybridization effects similar to those discussed in Ref. [34].

The electronic reconstruction is also revealed by structural distortions. After relaxation of the atomic positions, the apical O atom connecting the  $\text{TiO}_2$  and  $\text{NiO}_2$  layers is found to move about  $0.05$  Å towards the Ti atom, so that the apical Ni-O bond length is  $2.01$  Å and the Ti-O bond is  $1.91$  Å, as expected if charge is transferred from Ti to Ni. The in-plane Ti-O and Ni-O bond lengths are, on the other hand, much closer to each other and to the average of the apical bond lengths:  $1.96$  Å versus  $1.94$  Å. We therefore have an unusual situation of a large Jahn-Teller-type distortion about nominally spherical Ni ( $S = 1$ ) and Ti ( $S = 0$ ) ions. In addition to the bond lengths, the bond angles are also different from the bulk values. In the superlattice, the Ni-O-Ni bond angle is found to be  $157^\circ$ , compared to the bulk values of  $165^\circ$  (experiment [35]) and  $168^\circ$  (theory [36]). The decreased Ni-O-Ni bond angle reduces the in-plane inter-Ni hopping and helps stabilize the Mott insulating state. Both the bond lengths and bond angles have a weak dependence on  $U$ ; the numbers cited here are obtained from calculations at  $U_{\text{Ni}} = 6$  eV and  $U_{\text{Ti}} = 4$  eV,

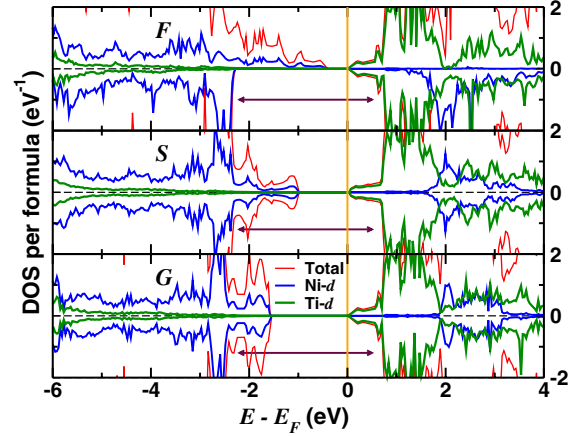


FIG. 4 (color online). Comparison of densities of states for ferromagnetic ( $F$ ), stripe antiferromagnetic ( $S$ ), and checkerboard ( $G$ ) magnetic orderings calculated at  $U_{\text{Ni}} = 6$  eV and  $U_{\text{Ti}} = 4$  eV. The conduction band minimum is aligned (highlighted by the orange line). The energy gap between the conduction band minimum and Ni  $d$  main peak (denoted by the maroon arrow) is approximately the same for different magnetic orderings.

but the  $0.1$  Å difference between the apical Ni-O and Ti-O bond lengths and a significantly decreased Ni-O-Ni bond angle are found at all the  $U$  values studied.

Within the DFT +  $U$  approximation for a wide range of  $U_{\text{Ni}}$ , we have studied three locally stable states: ferromagnetic ( $F$ ), stripe ( $S$ ) antiferromagnetic ordering [in-plane wave vector  $(0, 1/2)$ ] and checkerboard ( $G$ ) antiferromagnetic ordering [in-plane wave vector  $(1/2, 1/2)$ ]. Panel (a) of Fig. 3 shows the energy differences between these three states. We see that at all values of  $U_{\text{Ni}}$  the  $G$ -type antiferromagnetism has the lowest energy. As  $U_{\text{Ni}}$  becomes greater than  $1$  eV, the energy differences decrease, consistent with the notion that the  $\text{NiO}_2$  planes are in a Mott insulating state for which the magnetic energies scale as  $J \sim t^2/U$ .

Panel (b) of Fig. 3 shows the fundamental energy gap of the superlattice (which, as seen from the upper left panel of Fig. 1(c), is the energy difference between Ni  $d$  states and Ti  $d$  states). We see that in all cases, the fundamental gap increases linearly with  $U_{\text{Ni}}$  and with the same slope, indicating that the nature of the magnetic order only affects the onset of insulating behavior and not the basic properties of the state, again consistent with the idea that a Mott insulator has been created. Further insight into this phenomenon comes from the densities of states shown in Fig. 4. We see that changing the nature of the magnetic ordering modifies the details of the highest occupied states, but does not affect basic features such as the energy splitting between the Ni  $d$  main peak (Ni  $t_{2g}$  states) and Ti  $d$  states (conduction band minimum), as highlighted by the maroon arrow in Fig. 4. Panel (c) of Fig. 3 shows the magnetic moment on the Ni  $d$  site (computed using the VASP default atomic projector for Ni—see Supplemental Material [31]). We see that for  $U_{\text{Ni}} \geq 2$  eV, the magnitude of the local

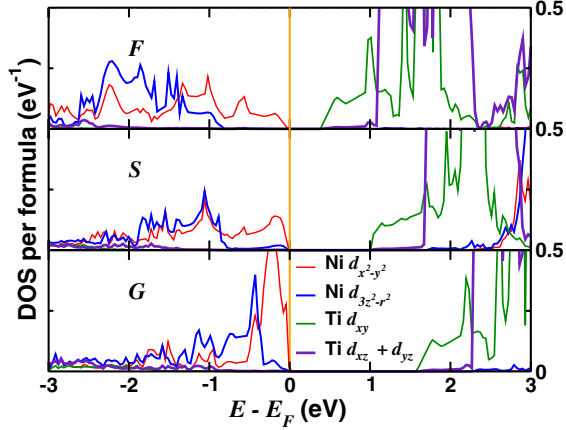


FIG. 5 (color online). Orbitaly resolved Ni  $e_g$  and Ti  $t_{2g}$  densities of states (red: Ni  $d_{x^2-y^2}$ ; blue: Ni  $d_{3z^2-r^2}$ ; green: Ti  $d_{xy}$ ; purple: Ti  $d_{xz} + d_{yz}$ ), computed at  $U_{\text{Ni}}=6\text{eV}$  and  $U_{\text{Ti}}=4\text{eV}$  for ferromagnetic ( $F$ ), stripe antiferromagnetic ( $S$ ) and checkerboard antiferromagnetic ( $G$ ) orderings.

magnetic moment is essentially independent of the nature of the ordering, is weakly  $U$  dependent, and is close to the value expected for the naive atomic  $S = 1$  states, once again confirming the Mott nature of the state predicted here.

To this point, our calculations have used the physically accepted value  $U_{\text{Ti}} = 4\text{eV}$  [32]. We have investigated the robustness of our results to the choice of  $U$  by sweeping the phase space spanned by  $U_{\text{Ti}}$  and  $U_{\text{Ni}}$  for the  $F$ ,  $S$ , and  $G$  magnetic states. We find the energy sequence  $G < S < F$  throughout the phase space. Figure 3(d) shows that although the position of the metal-insulator transition boundaries depends on the  $U$  values, the essential features are  $U$  independent. The phase boundary for all the magnetic states has a negative slope, which is understood as follows: within DFT +  $U$ ,  $U_{\text{Ti}}$  increases the Ti  $t_{2g}$  states because the Ti  $t_{2g}$  shell is less than half filled, while  $U_{\text{Ni}}$  increases the energy gap between the Ni  $e_g$  majority and minority spins. Therefore, with a given  $U_{\text{Ti}}$ , we need a  $U_{\text{Ni}}$  large enough to separate Ni  $e_g$  and Ti  $t_{2g}$  states and open a fundamental gap and vice versa. With  $U_{\text{Ni}}$  6 eV or larger, Mott physics dominates, as the system is rendered insulating for all the magnetic orderings and all the values of  $U_{\text{Ti}}$ .

The most important experimental test of our calculations is that the superlattice should be a quasi-two-dimensional  $S = 1$  magnetic insulator, with the moments residing on the Ni sites and the correlations most likely antiferromagnetic. The position of the apical oxygen (nearer to the Ti than the Ni) and the reduced Ni-O-Ni bond angle are other important indicators of the predicted electronic reconstruction. Orbital splitting is also a test of our calculations. Figure 5 presents the orbitaly resolved densities of states for a representative case ( $U_{\text{Ni}} = 6\text{eV}$  and  $U_{\text{Ti}} = 4\text{eV}$ ). In the majority spin channel both Ni  $d_{x^2-y^2}$  and  $d_{3z^2-r^2}$  orbitals are occupied, leading to a spin  $S = 1$  configuration, while all Ti  $t_{2g}$  orbitals are empty, resulting in a spin

$S = 0$  configuration. Since both Ni  $e_g$  orbitals are filled and all of the three Ti  $t_{2g}$  orbitals are empty, there is no orbital polarization in the sense of Refs. [37,38]. However, our first-principles calculations show that the valence band maximum is mainly of Ni  $d_{x^2-y^2}$  character and the conduction band minimum is dominantly of Ti  $d_{xy}$  character. This orbital ordering indicates that small hole doping may lead to an orbitally selective Mott metallic state [39,40] with a single orbital (Ni  $d_{x^2-y^2}$ ) active at the Fermi surface but coupled to antiferromagnetically correlated spins on the Ni  $d_{3z^2-r^2}$  orbitals. In this case, the carriers' motion is strongly affected by magnetism, which is similar to  $\text{La}_{2-x}\text{Sr}_x\text{NiO}_4$ . However, on the other hand, small electron doping may result in a Ti  $d_{xy}$  single orbital Fermi surface, in which the carriers are only weakly coupled to the antiferromagnetic ordering in the  $\text{NiO}_2$  layer. This feature is absent in conventional doped Mott insulators. The comparison of the carriers' strong or weak coupling to correlated spins in one system poses an interesting open question and remains to be explored in experiment. Resonant x-ray photoemission may shed light on the fundamental differences between these predicted phases.

In conclusion, we have shown within the DFT +  $U$  approximation that in a  $(\text{LaTiO}_3)_1/(\text{LaNiO}_3)_1$  superlattice, correlation effects are greatly enhanced on the Ni sites, producing a  $S = 1$  Mott insulator with an unusual charge transfer gap set by Ni  $d$  and Ti  $d$  states, distinct from conventional Mott insulators. The superlattice structure leads to a single orbital character at band edges and indicates interesting new physics with carrier doping, which is absent in double perovskites. We believe that DFT +  $U$  approximation provides a reliable description of correlation effects for stoichiometric and ordered materials. More sophisticated methods (e.g., DFT + dynamical mean field theory) might be needed to treat doped systems with mobile carriers. Our findings open a new direction for the control of correlation effects via charge transfer and heterostructuring in perovskite oxides.

We thank Charles Ahn and Sohrab Ismail-Beigi for helpful conversations. This research was supported by the Army Research Office under ARO-Ph 56032 and the U.S. Department of Energy under Grant No. DOE-ER-046169. Computational facilities are provided via XSEDE resources through Grant No. TG-PHY130003. Additional computational resources are provided by the facilities and staff of the Yale University Faculty of Arts and Sciences High Performance Computing Center, supported by NSF Grant No. CNS 08-21132.

- 
- [1] H. Hwang, Y. Iwasa, M. Kawasaki, B. Keimer, N. Nagaosa, and Y. Tokura, *Nat. Mater.* **11**, 103 (2012).
  - [2] A. Ohtomo, D. A. Muller, J. L. Grazul, and H. Y. Hwang, *Nature (London)* **419**, 378 (2002).

- [3] A. Ohtomo and H. Y. Hwang, *Nature (London)* **427**, 423 (2004).
- [4] S. Thiel, G. Hammerl, A. Schmehl, C. W. Schneider, and J. Mannhart, *Science* **313**, 1942 (2006).
- [5] N. Reyren *et al.*, *Science* **317**, 1196 (2007).
- [6] A. D. Caviglia, S. Gariglio, N. Reyren, D. Jaccard, T. Schneider, M. Gabay, S. Thiel, G. Hammerl, J. Mannhart, and J. M. Triscone, *Nature (London)* **456**, 624 (2008).
- [7] A. D. Rata, A. Herklotz, K. Nenkov, L. Schultz, and K. Dörr, *Phys. Rev. Lett.* **100**, 076401 (2008).
- [8] K. Yoshimatsu, T. Okabe, H. Kumigashira, S. Okamoto, S. Aizaki, A. Fujimori, and M. Oshima, *Phys. Rev. Lett.* **104**, 147601 (2010).
- [9] J. Chakhalian *et al.*, *Phys. Rev. Lett.* **107**, 116805 (2011).
- [10] R. Scherwitzl, S. Gariglio, M. Gabay, P. Zubko, M. Gibert, and J.-M. Triscone, *Phys. Rev. Lett.* **106**, 246403 (2011).
- [11] H. W. Jang *et al.*, *Science* **331**, 886 (2011).
- [12] A. V. Boris *et al.*, *Science* **332**, 937 (2011).
- [13] A. Brinkman, M. Huijben, M. V. Zalk, J. Huijben, U. Zeitler, J. C. Maan, W. G. V. der Wiel, G. Rijnders, D. H. A. Blank, and H. Hilgenkamp, *Nat. Mater.* **6**, 493 (2007).
- [14] L. Li, C. Richter, J. Mannhart, and R. C. Ashoori, *Nat. Phys.* **7**, 762 (2011).
- [15] J. A. Bert, B. Kalisky, C. Bell, M. Kim, Y. Hikita, H. Y. Hwang, and K. A. Moler, *Nat. Phys.* **7**, 767 (2011).
- [16] J. Liu, S. Okamoto, M. van Veenendaal, M. Kareev, B. Gray, P. Ryan, J. W. Freeland, and J. Chakhalian, *Phys. Rev. B* **83**, 161102 (2011).
- [17] J. Liu, M. Kareev, D. Meyers, B. Gray, P. Ryan, J. W. Freeland, and J. Chakhalian, *Phys. Rev. Lett.* **109**, 107402 (2012).
- [18] H. Chen, D. P. Kumah, A. S. Disa, F. J. Walker, C. H. Ahn, and S. Ismail-Beigi, *Phys. Rev. Lett.* **110**, 186402 (2013).
- [19] E. J. Monkman, C. Adamo, J. A. Mundy, D. E. Shai, J. W. Harter, D. Shen, B. Burganov, D. A. Muller, D. G. Schlom, and K. M. Shen, *Nat. Mater.* **11**, 855 (2012).
- [20] J. Chakhalian, J. W. Freeland, H.-U. Habermeier, G. Cristiani, G. Khaliullin, M. van Veenendaal, and B. Keimer, *Science* **318**, 1114 (2007).
- [21] J. Chakhalian *et al.*, *Nat. Phys.* **2**, 244 (2006).
- [22] J. Garcia-Barriocanal *et al.*, *Nat. Commun.* **1**, 82 (2010).
- [23] M. Gibert, P. Zubko, R. Scherwitzl, J. Iniguez, and J.-M. Triscone, *Nat. Mater.* **11**, 195 (2012).
- [24] J. Hoffman, I. C. Tung, B. Nelson-Cheeseman, M. Liu, J. Freeland, and A. Bhattacharya, [arXiv:1301.7295](https://arxiv.org/abs/1301.7295) [Phys. Rev. B (to be published)].
- [25] A. T. Lee and M. J. Han, *Phys. Rev. B* **88**, 035126 (2013).
- [26] D. Serrate, J. M. D. Teresa, and M. R. Ibarra, *J. Phys. Condens. Matter* **19**, 023201 (2007).
- [27] N. Rogado, J. Li, A. Sleight, and M. Subramanian, *Adv. Mater.* **17**, 2225 (2005).
- [28] K. Holmana, Q. Huang, T. Klimczuk, K. Trzebiatowski, J. Bos, E. Morosan, J. Lynn, and R. Cava, *J. Solid State Chem.* **180**, 75 (2007).
- [29] J. Chaloupka and G. Khaliullin, *Phys. Rev. Lett.* **100**, 016404 (2008).
- [30] P. Hansmann, X. Yang, A. Toschi, G. Khaliullin, O. K. Andersen, and K. Held, *Phys. Rev. Lett.* **103**, 016401 (2009).
- [31] See Supplemental Material at <http://link.aps.org/supplemental/10.1103/PhysRevLett.111.116403> for the technical details of calculation.
- [32] T. Mizokawa and A. Fujimori, *Phys. Rev. B* **51**, 12880 (1995).
- [33] S. Okatov, A. Poteryaev, and A. Lichtenstein, *Europhys. Lett.* **70**, 499 (2005).
- [34] C. A. Marianetti, G. Kotliar, and G. Ceder, *Phys. Rev. Lett.* **92**, 196405 (2004).
- [35] J. B. Torrance, P. Lacorre, A. I. Nazzari, E. J. Ansaldo, and C. Niedermayer, *Phys. Rev. B* **45**, 8209 (1992).
- [36] G. Gou, I. Grinberg, A. M. Rappe, and J. M. Rondinelli, *Phys. Rev. B* **84**, 144101 (2011).
- [37] E. Benckiser *et al.*, *Nat. Mater.* **10**, 189 (2011).
- [38] M. J. Han, X. Wang, C. A. Marianetti, and A. J. Millis, *Phys. Rev. Lett.* **107**, 206804 (2011).
- [39] V. I. Anisimov, I. A. Nekrasov, D. E. Kondakov, T. M. Rice, and M. Sgrist, *Eur. Phys. J. B* **25**, 191 (2002).
- [40] L. de' Medici, S. R. Hassan, M. Capone, and X. Dai, *Phys. Rev. Lett.* **102**, 126401 (2009).